Journal of Computational and Applied Mathematics 474 (2026) 116966

Contents lists available at ScienceDirect

Journal of Computational and Applied Mathematics

journal homepage: www.elsevier.com/locate/cam

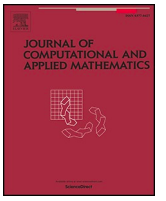

A numerical study on flow velocities, bed morphology and suspended sediment transport due to barge motion in a navigation channel

Nuray Gedik [a,*], Onur Bora [b], M. Adil Akgül [c], Mehmet Sedat Kabdaşlı [d], Emel İrtem [e]

[a] Department of Civil Engineering, Balikesir University, Balikesir 10145, Türkiye
[b] Department of Science Affairs, Balikesir Metropolitan Municipality, Balikesir 10185, Türkiye
[c] Department of Civil Engineering, Turkish-German University, Istanbul, 34820, Türkiye
[d] Formerly at the Faculty of Civil Engineering, Istanbul Technical University, Istanbul 34672, Türkiye
[e] Department of Civil Engineering, Doğuş University, Istanbul 34775, Türkiye

ARTICLE INFO

Keywords:
Navigation channel
Sediment transport
Sediment suspension
Computational fluid dynamics
Numerical modelling

ABSTRACT

Sediment suspension and motion due to vessel traffic in navigation channels is a challenging problem in the design and management of waterways, ports and navigation channels. This study utilised computational fluid dynamics (CFD) simulations to investigate the impact of vessel motion on bed morphology and sediment suspension. The work was carried out for a navigation channel with sloped banks, subject to motion-induced currents and waves generated by a rectangular barge with a blunt bow, towed at constant speed. A fine sand channel bottom was modelled. The simulations, consisting of six different scenarios with two bank slope angles, two tow speeds and two vessel widths, have been carried out by FLOW-3D Hydro software. It was found out that the most significant parameter affecting sediment motion is the tow speed of the vessel, which is coupled with the vessels squat. The study further shows that ship width also plays a critical role in predicting the risk of sediment accumulation in harbour and navigation channel projects, as an increase of only 15 % in vessel width results in a large increase of 72 % in the total amount of suspended sediment. An increase in bank slopes, on the other hand, is found to have a smaller effect (15 %) on the total suspended sediment concentration.

1. Introduction

The evolution of computers during the last decades has boosted the utilization and implementation of CFD into a vast number of engineering and scientific problems. Recent advances in fluid dynamics modeling, particularly involving fractional calculus and complex geometries, have provided deeper insights into various flow phenomena relevant to channel hydrodynamics. For instance, fractional models have been successfully applied to describe fluid transport in porous and non-porous media under magnetic fields [1], offering a framework that could potentially be extended to sediment-laden flows in engineered channels. Similarly, studies on peristaltic flow in rotating and wavy channels for non-Newtonian fluids [2] highlight the importance of geometric complexity and fluid rheology—factors that are also crucial in vessel-induced flow disturbances near sloped banks. Moreover, fractional wave-like

* Corresponding author.
E-mail addresses: ngedik@balikesir.edu.tr (N. Gedik), bora.onur@gmail.com (O. Bora), mehmetadil.akgul@tau.edu.tr (M.A. Akgül), kabdaslim@gmail.com (M.S. Kabdaşlı), eirtem@dogus.edu.tr (E. İrtem).

https://doi.org/10.1016/j.cam.2025.116966
Received 5 April 2025; Received in revised form 7 July 2025;
Available online 21 July 2025

equations defined on radially symmetric domains [3] underscore the versatility of fractional approaches in modeling wave propagation and resonance effects, which are relevant to understanding vessel-generated waves and their influence on bed morphology. These advanced mathematical models may enhance the predictive capabilities of CFD-based simulations in future research on sediment transport for a vast variety of channels conveying different fluids and multiphased media. A typical example of such interesting solid-liquid problem arises in waterways and navigation channels due to induction of sediment motion by vessels passing through.

The tonnage of international maritime transport is growing every year. It has been reported that the annual growth of the tonnage of the cargo transported by maritime routes is increasing at a rate of 2.4 % per annum [4]. Besides increasing the density of marine traffic, another consequence is observed as the size increase of merchant fleet vessels. Thus, provision of navigational safety becomes a challenging mission for both port authorities and waterway engineers, boosting in confined and shallow waterways. A specific form of shallow and confined waterways are navigation channels, providing the sole access routes for many marine vehicles to coastal and inland ports and ports adjacent to rivers. The increase in marine traffic and vessel sizes lead to a rise in morphological changes in navigation channels caused by vessel motion, which may reduce operational safety and can further lead to environmental problems.

The motion of a vessel in a navigation channel is a complex phenomenon including the vessel properties, channel properties and environmental factors such as winds, waves, and currents. The geometry of the vessel, its mass distribution, and its propulsion systems dictate its motion properties and generate disturbances in the surrounding water, including waves, propeller jets, and squat. The action of environmental parameters such as wind, waves, and current are imposed as parameters disturbing the equilibrium of the vessel in a calm fluid, generating changes in vessel heading and speed and also inducing wave-induced motions such as heave and roll. The channel, on the other hand, is characterized by its geometry, made of its length, depth and cross section properties, and the properties of the material covering its banks and bottom. Especially in wide channels, mainly due to economical issues, the bottom of a channel is usually covered with existing bed material, being usually fine such as silt and sand, prone to motion due to its low stability. Motion of bottom material leads to sediment transport along or across the channel and consequently to the generation of bottom irregularities, which may cause a threat to a high draft vessel. Thus, monitoring and lining/dredging works in such channels to maintain bed stability are common works, composing a significant amount of their management costs.

Sediment motion in navigation channels and waterways may be caused by different phenomena such as waves, currents, and ship motion. From these parameters, ship motion has been vastly studied in the discipline of naval architecture, including ship generated waves, seakeeping studies and the fluid-vessel interaction during movement. A significant feature during vessel motion, in particular for this study, is defined as the squat. A vessel moving in a fluid pushes the water at the bow forward, which is displaced to the keel and boards of the ship to reach equilibrium. Consequently, flow velocities increase around the vessel, leading to a pressure drop and hence generating a force acting downward. . This downward movement of the vessel continues until equilibrium is restored. This phenomenon is referred to as squat [5]. Usually becoming greater at the bow of the vessel, squat is proportional to the square of vessel speed and in addition to decreasing manoeuverability, it can also lead to unpredicted accidents in confined or shallow waters such as grounding. In a similar manner to shallow waters, squat increases when a vessel is travelling in a channel, due to increased confinement. For such cases, squat can be predicted by a number of empirical equations. PIANC (2014) indicates the parameters acting on the squat value of a vessel moving in a navigation channel as the type and cross section geometry of the channel, channel depth, channel slope, vessel draft, blockage coefficient, backflow coefficient, depth Froude number and critical vessel speed [6] and recommends seven different case-specific equations for its prediction. In this study, following PIANC equation has been used for the prediction of squat, which is derived from the study of Tuck [7]:

$$S = C_S \frac{\nabla}{L_{BP}^2} \frac{F_R^2}{\sqrt{(1 - F_R^2)}} \tag{1}$$

In this context, S denotes the value of squat in meters, C_S is the Huuska-Guliev coefficient (2.4 for a box-shaped hull), L_{BP} is the length of the vessel between peak perpendiculars, which is equivalent to the length over all (L_OA) for a box-shaped barge, ∇ is the displacement volume of the vessel and F_R is the Froude number.

The pattern of waves and currents generated due to ship motion are also extensively studied in the literature. For a more comprehensive overview of this subject, readers are directed to consult Bora [8].

While a vast number of studies and guidelines are available for the wave- and current- induced sediment motion, studies dealing with the effect of vessel motion on sediment transport are rare. A recent publication about the design of navigation channels and related sediment problems has been prepared by ASCE [9], where a comprehensive overview of the interaction between the channel geometry, traffic and environmental factors on sedimentation problems has been presented. A group of studies about the effect of vessel waves on sediment motion consider only the marine traffic and consequently arising shoreline and bottom topography changes, the majority of which are based on site measurements. Ravens [10] pointed out the significance of high-frequency ship waves in sediment transport in Boston Harbor and Dorchester Bay. Vessel-induced forces and their effect on sediment transport and sediment suspension has been researched by Maynord [11]. A method for the prediction of suspended sediment concentrations due to ship waves for both cohesive and non-cohesive bottom materials has been developed by Parchure et al. [12]. Bauer et al. [13] found out that a strong correlation exists between boat wakes and levee erosion in the Sacramento-San Joaquin Delta. Suspended sediment concentrations due to vessel motion in regions with limited fetch lengths such as rivers and sheltered channels, acc. to McConchie and Toleman [14], can be 80 times greater than the wave induced case. This finding is also supported by Houser [15] for narrow channels. The effect of vessel-induced suspended sediment concentration on environmental parameters has been studied by Eriksson et al. [16] for aquatic vegetation in the Stockholm archipelago, Baltic Sea; pointing out that changes in bottom morphology significantly affect biodiversity and aquatic vegetation growth in deeper waters. The effects of marine traffic in the Venice Lagoon has been studied by

Rapaglia et al. [17], who indicate that suspension times can increase up to one hour due to dense marine traffic, leading to adverse effects in water quality and aquatic life. The shoreline erosion due to marine traffic has been investigated by Zaggia et al. [18] for Malamocco-Marghera Canal in the Venice Lagoon, who point out the primary reason for the erosion as the heavy marine traffic, leading to an annual shoreline recession of 3–4 m per annum. Duro et al. [19] investigated vessel-induced morphological changes in Meuse River, Netherlands with an emphasis kept on bank erosion and channel bed alterations. Mao and Chen [20] studied vessel induced wave and current data due to marine traffic in Grand Canal, Jiangsu, China, concluding that the dense marine traffic vastly increases bed flow velocities up to nine times during the passage of a vessel.

Studies addressing the effect of vessel motion on sediment movement in channels and waterways, with an insight kept on vessel characteristics and vessel-induced forces and currents also exist. For this purpose, physical and numerical models have been used. The effect of ships with and without propellers on suspended sediment concentrations has been studied by Ji et al. [21,22] with a 3D physical model study. The effect of channel width, water depth and ship draft is researched with towing tests for inland convoys in a physical model environment by Du et al. [23], who indicate that the ship resistance increases with decreasing channel width, increasing vessel beam and decreasing channel depth, hence affecting sediment resuspension. The flow velocities and pressures on the seabed due to ship motion are studied by Robjins [24] through physical model tests, pointing out that the bow shape and the keel clearance of the most critical parameters affecting flow velocities. A full-scale physical model test has been carried out by Schroevers et al. [25] by using a deeply loaded barge in the Juliana Canal, Netherlands; pointing out a significant erosion in the canal bed with sediment moving towards the channel banks through each vessel passage.

Though the motion of a powered or non-powered vessel in confined waters induce sediment motion, other oceanographical or hydrological parameters also affect sediment resuspension and bed morphology. For instance, the effect of hydrological parameters on an estuarine navigation channel have been pointed out by Silva et al. [26] carried out a field study in the Porto Novo basin and access channel in Patos Lagoon Estuary, Southern Brazil. A study carried out by Muscalus and Haas [27] used data achieved from pressure sensors deployed along the Main Channel at Bird/Long Island, Savannah River, Georgia, where data is separated with respect to their triggering forces. The study points out that the majority of the morphological changes occurring along the channel is causes by ship waves.

A numerical model study has been carried out by Colangeli et al. [28] about the effect of propeller jet flow on sediment transport for both stationary and moving vessels. The study indicates that the sediment in suspension dominates the morphological changes in the seabed for the case of moving vessels contrary to the bed load prevalence for vessels at zero speed, pointing out the importance of hull effect and related sediment motion.

The literature review presented above indicates that although the topic of vessel-induced sediment transport has been studied extensively, it has not been refined to evaluate the relationships between the individual channel physical parameters (width, depth, bank slopes, bed material etc.) and operational parameters (tow speed, clearance height, propulsion type etc.) governing the phenomena. It is thought that the individual interactions of these parameters and the abilty of their prediction can be useful in the design and management of navigation channels and waterways, and also it can be helpful in the mitigation of environmental impacts. For this purpose, a study has been carried out by Gedik et al. [29] inspecting the hydro- and morpho-dynamics on a channel bed for a barge under tow with blunt- and raked bow configurations over a flat bed, where also a multivariate regression model has been used to predict sediment motion under different cases. This study is a further expansion of the work mentioned above, and focuses on the channel geometry, to which banks with different slope angles are introduced. Computational Fluid Dynamics simulations have been used for the study in FLOW-3D Hydro commercial software with the details described in the following sections.

2. Materials and methods

The study has been carried out by utilizing the commercial FLOW-3D Hydro software developed by Flow Science, Inc. In FLOW-3D Hydro, the continuity Eq. (2) is solved by a finite volume approach, whereas the motion of the fluid is evaluated by unsteady Reynolds-averaged Navier-Stokes (RANS) equations in (3–4) [30].

$$\frac{\partial}{\partial X_i} U_i A_i = 0 \tag{2}$$

$$\frac{\partial U_i}{\partial t} + \frac{1}{V_f}\left(U_j A_j \frac{\partial u}{\partial X_j}\right) = -\frac{1}{\rho}\frac{\partial P}{\partial X_i} + G_i + f_i \tag{3}$$

$$\rho V_f f_i = \tau_{b,i} - \left[\frac{\partial}{\partial X_j}\left(A_j S_{ij}\right)\right];\ S_{ii} = -2\mu_{tot}\left[\frac{\partial U_i}{\partial X_i}\right];\ S_{ij} = -\mu_{tot}\left[\frac{\partial U_i}{\partial X_j} + \frac{\partial U_j}{\partial X_i}\right] \tag{4}$$

In (2–4), t is time, U_i is the mean velocity, A_i is the fractional area of the flow in i-direction, P is pressure, V_f is the fractional volume of the flow. G_i represents body accelerations, f_i represents viscous accelerations, S_{ij} is the strain rate tensor, $\tau_{b,i}$ is the bottom shear stress, ρ is the density of water and μ_{tot} is the total viscosity represented as the sum of dynamic viscosity μ and the turbulence (eddy) viscosity μ_T.

Modelling of sediment transport necessitates the adoption of a good turbulence model in order to maintain accuracy for the prediction of the near-wall shear stresses. Six different turbulence models are embedded into FLOW-3D, which can be counted as the Prandtl mixing length model, one-equation k-ε model, two-equation k-ε model, renormalization group model (RNG), k-ω model and large eddy simulation (LES). RNG models [31] are reported for their highly accurate estimations in low intensity turbulence flows and

flows with strong shear regions. An RNG model closely resembles the k-ε model, but equation constants in an RNG model are derived explicitly, whereas they are found empirically in a k-ε model. The equations for the RNG turbulence model are given below:

$$\frac{\partial(\rho k)}{\partial t}+\frac{\partial(\rho k u_i)}{\partial x_i}=\frac{\partial}{\partial x_j}\left[\left(\mu+\frac{\mu_T}{\sigma_k}\right)\frac{\partial k}{\partial x_j}\right]+P_k-\rho\varepsilon \tag{5}$$

$$\frac{\partial(\rho\varepsilon)}{\partial t}+\frac{\partial(\rho\varepsilon u_i)}{\partial x_i}=\frac{\partial}{\partial x_j}\left[\left(\mu+\frac{\mu_T}{\sigma_\varepsilon}\right)\frac{\partial(\varepsilon)}{\partial x_j}\right]+C_{1\varepsilon}\frac{\varepsilon}{k}P_k-C_{2\varepsilon}\rho\frac{\varepsilon^2}{k} \tag{6}$$

In (5–6), k is the turbulence kinetic energy, ε is the dissipation rate, x_i denotes the distance in the i-axis and P_k is the production of turbulence kinetic energy due to mean velocity gradients. Here, the default values of σ_k and σ_ε are taken as 1.39. For the coefficients $C_{1\varepsilon}$ and $C_{2\varepsilon}$, default values of 1.42 and 1.68 are assigned, respectively. For the calculation of turbulent viscosity, in (7) is used with the parameter C_μ assigned as 0.85.

$$\mu_T=\rho C_\mu\frac{k^2}{\varepsilon} \tag{7}$$

Modelling of the sediment suspension is treated by adopting the model based on Mastbergen and Van den Berg [32]. In order to estimate sediment motion, the critical Shields parameter should be calculated, initiating with the calculation of the dimensionless parameter $d_{*,i}$:

$$d_{*,i}=d_i\left[\frac{\rho_f(\rho_i-\rho_f)\parallel g\parallel}{\mu_f^2}\right]^{1/3} \tag{8}$$

In (8), d_i is the median sediment diameter for species i, ρ_i is the density of the sediment species i, ρ_f is the density of the fluid, μ_f is the fluids dynamics viscosity and g is the gravitational acceleration. The dimensionless critical Shields parameter is calculated by using Soulsby-Whitehouse Eq. (9).

$$\theta_{cr,i}=\frac{0.3}{1+1.2d_{*,i}}+0.055\left[1-exp\left(-0.02d_{*,i}\right)\right] \tag{9}$$

Regarding sloping surfaces, in (9) is modified, including the angle of repose (10):

$$\theta'_{cr,i}=\theta_{cr,i}\frac{\cos\psi\sin\beta+\sqrt{\cos^2\beta\ tan^2\varphi_i-sin^2\psi sin^2\beta}}{tan\varphi_i} \tag{10}$$

In (10), ψ is the angle between the flow direction and the upslope direction, β is the bed slope angle and φ is the angle of repose for the bed material. Local bed shear stress has been used to compute the local Shields parameter, defined by (11).

$$\theta_i=\frac{\tau}{\parallel g\parallel d_i(\rho_i-\rho_f)} \tag{11}$$

In (11), the local bed shear stress is computed by using the law of the wall and the quadratic bottom shear stress law for 3D shallow water turbulent flow, where the bed surface roughness is also taken into account. For the settling velocity, Soulsby equation [33] is used (12):

$$u_{set,i}=\left[\left(10.36^2+1.049d_*^3\right)^{0.5}-10.36\right] \tag{12}$$

The volumetric rate of bed load transport per unit width of the bed is calculated by (13):

$$\Phi_i=\beta_{VT,i}d_{*,i}^{-0.3}\left(\frac{\theta_i}{\theta'_{cr,i}}-1.0\right)^{2.1}c_{b,i} \tag{13}$$

In (13), the coefficient $\beta_{VT,i}$ is taken as 0.053. The parameter $c_{b,i}$ denotes the volumetric fraction of species in the bed material. The suspended sediment concentration is calculated for each species by solving its corresponding transport Eq. (14):

$$\frac{\partial C_{s,i}}{\partial t}+\nabla.\left(u_{s,i}C_{s,i}\right)=\nabla.\nabla\left(DC_{s,i}\right) \tag{14}$$

In (14), $C_{s,i}$ is the suspended sediment mass concentration of sediment species i, i.e. the mass of the sediment per unit volume of the fluid-sediment mixture. D denotes diffusivity and $u_{s,i}$ is the velocity of the suspended sediment.

The geometry definition has been carried out by using the FAVOR (Fractional Area/Volume Obstacle Representation) method. In the FAVOR method, the cells adjacent to any solid boundary are not limited by the actual solid boundary, they may protrude in the boundary normal direction past the boundary. Hence the net flow areas are defined as the fractional area of the actual flow areas to the total grid size; these are called as the fractional areas. In three dimensions, it leads to the generation of fractional volumes. The mesh generation consequently is greatly simplified without having any effect on the accuracy of the results.

In order to track the fluid interfaces, Volume-of-Fluid (VOF) method presented by Hirt and Nichols [34] can be used. This algorithm

is used in FLOW-3D to determine the free surface of the flow. In VOF method, the fluid volume in any grid cell is defined as the ratio F of the fluid volume to the grid cell volume. Thus, a grid cell occupied entirely by the fluid such as a cell in the flow field yields the F value of 1.0, whereas a grid cell outside the flow field has an F value of 0.0. The free surface, i.e. the liquid-gas (air) interface is evaluated along the boundary which is supposed to be partially filled with fluid, an F value between 0.0 and 1.0 is obtained (15):

$$\frac{\partial F}{\partial t}+\frac{\partial F}{\partial X}+\frac{\partial F}{\partial Y}+\frac{\partial F}{\partial Z}=0 \tag{15}$$

3. Model setup

3.1. Vessel and navigation channel

In order to pick convenient dimensions for the vessel, which has been chosen as a barge without any engine, a market study has been carried out, covering a total number of 40 commercial barges [8]. Based on this inspection, a blunt-bow barge with dimensions of $L_{OA} = 15$ m and $d = 2$ m has been selected. Two different widths of $B = 6$ m and $B = 6.9$ m have been used in the model for the inspection of vessel width. The isometric view and dimensions of the barge are shown in Fig. 1.

The draft of the model has been adjusted by changing the global density of the barge in order to attain the desired spacing between the keel of the barge and the seabed. For all the scenarios carried out in this study, a constant draft of 1.60 m has been selected.

General Moving Object (GMO) method of FLOW-3D has been used to introduce the motion of the barge in this study. GMO enables to define the motion of a floating object either by a pre-defined motion path or as a flow-coupled dynamic object movement in up to six degrees of freedom. For the case of flow-coupled motion, external forces or moments acting on the floating object can also be defined, enabling realistic object-fluid interaction simulations. In this study, since the effect of environmental effects such as winds, waves, and currents are omitted, the motion of the barge is defined by a controlled approach. The barge will be towed with constant speed along the x-direction throughout all the scenarios. To achieve stability for vessel motion, the rotation around the z-axis has been constrained in order to hinder yaw motions. The translation along the y-axis has also been restricted to avoid lateral drift. In order to receive the barges natural responses to hydrodynamic forces during the scenario, translation along x- and z-axis and rotations around x- and y-axis have been left unconstrained.

The maximum velocity for the barge has been selected as $V = 2$ m/s (approx. 4 knots) in this study in order to calculate channel dimensions. In order to attain a realistic modeling environment, the recommendations of PIANC (2014) have been considered for the dimensioning of the navigation channel. Here, the aim is to evaluate the maximum possible hydro- and morphodynamic effects which may be allowed under existing design regulations. In this particular study, the squat value for the vessel for a maximum towing speed of 2 m/s has been calculated by (1) as $S = 0.45$ m By omitting unbalanced loading factor, wave factor (no waves are introduced during the simulations) and siltation depth, the depth of the channel has been selected as 2.05 m For the width of the channel, PIANC (2014) recommends the consideration of an extra width containing the effects of cross-wind, cross- and longitudinal currents, significant wave height, navigation assistance availability, channel bottom properties, vessel speed and loading deviations and passing distance. Since the effect of environmental forces such as wind and waves are neglected in this study, a channel width for a straight section in a protected water without these factors has been assigned. For this purpose, PIANC (2014) recommends a minimum width of 1.8B for the width of the basic manoeuvering lane considering poor manoeuvering conditions, i.e. vessel under tow. Consequently, a basic manoeuvering lane width of $B = 12$ m has been chosen. Two different bank slopes have been used; 1:3 and 1:5, respectively. The banks of the channel are left at a constant depth of 1.6 m The cross section dimensions of the navigation channel are shown in Fig. 2.

3.2. Computational domain

In order to achieve a stable numerical modelling environment, the dimensions of the computational domain must be selected in such a way that no disturbances due to domain boundaries disrupt the physical phenomena studied.

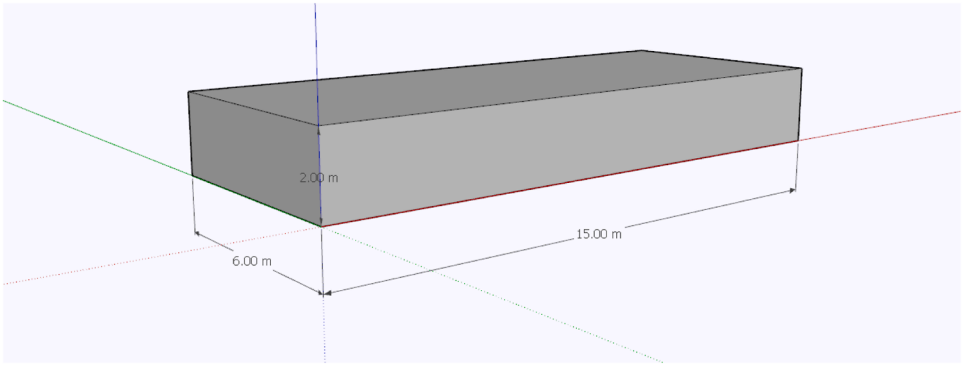

Fig. 1. Isometric view and dimensions of the barge.

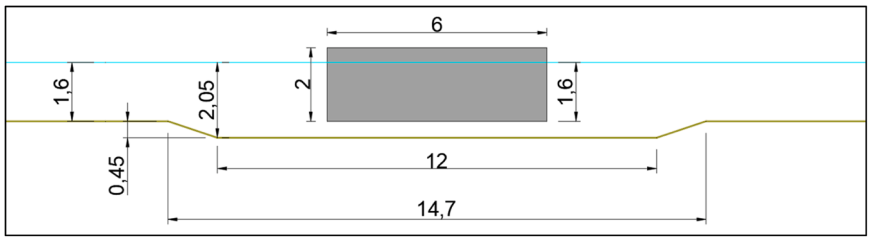

Fig. 2. Cross section of the navigation channel used in the studys (s = 1:3).

In this study, the barge will be towed with a constant acceleration until its towing speed, and will propagate further at a constant speed. For the propagation velocities, 1.0 m/s and 1.5 m/s have been selected. Accelerations were kept constant across all scenarios to eliminate differences in model results due to acceleration. The length of the computational domain is set to 100 m

A number of pilot tests have been carried out in order to determine the width of the numerical channel with the aim of preventing occurrence of secondary effects on hydro- and morphodynamic results caused by boundaries such as reflection of ship waves. It has been found out that a total channel width of 22 m is sufficient to hinder secondary effects. Consequently, a numerical domain width of 22 m has been assigned to the cases with 1:3 bank slopes. The width has been increased to 23.8 m for the cases with 1:5 bank slope in order to retain the sufficient width between the top edge of the bank and the domain boundary.

For the determination of the grid size, a sensitivity analysis has been carried out with different grid sizes and structures. A sufficient convergence has been achieved for a mesh with 0.15 m cubic cell dimensions, which has been refined to 0.0375 m near the channel bed (Fig. 3).

In order to depict the physics of the system accurately, boundary conditions must be defined accurately. Based on the physical requirements of each boundary, different boundary conditions are applied. The numerical channel is shown in Fig. 4 with its applied boundary conditions. In Fig. 4, A denotes the atmospheric condition, which is known as the free surface condition; this boundary condition has been applied along the intersection of water and open air. O denotes the outflow condition, indicating that no restrictions take place at this boundary, i.e. the flow continues beyond it. Outflow boundary condition has been applied to the minimum and maximum x-axis boundaries. For the minima and maxima of the y-axis boundaries, symmetry (S) boundary condition has been used for the derivation of an infinite wide domain and minimization of edge effects. At the bottom, wall (W) boundary condition has been applied, defining the interface of the fluid with a solid bottom.

For the modelling of the channel bed, a sediment with a median grain diameter of 0.0625 mm and a specific gravity of 2650 kg/m^3 has been used, representing fine sand. For this particular bed material, a bed-load transport coefficient of 0.06 and a drag coefficient of 0.018 have been assigned.

3.3. Simulation scenarios

A total of eight simulations have been carried out for the study, taking into account two different barge widths of B = 6.0 m and 6.9 m, two different towing speeds of V = 1.0 m/s and 1.5 m/s and two different bank slope angles of 1:3 and 1:5, respectively. The draft of the vessel is set to the constant value of 1.60 m in all scenarios, yielding a keel clearance of 0.45 m between the keel of the barge and the channel bottom. The scenarios utilized in the study are presented in Table 1.

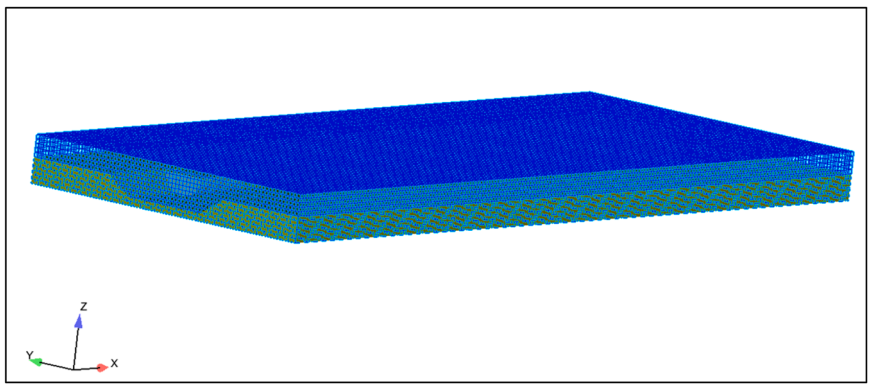

Fig. 3. 3D view of the grid structure (Model with 1:3 bank slopes is shown).

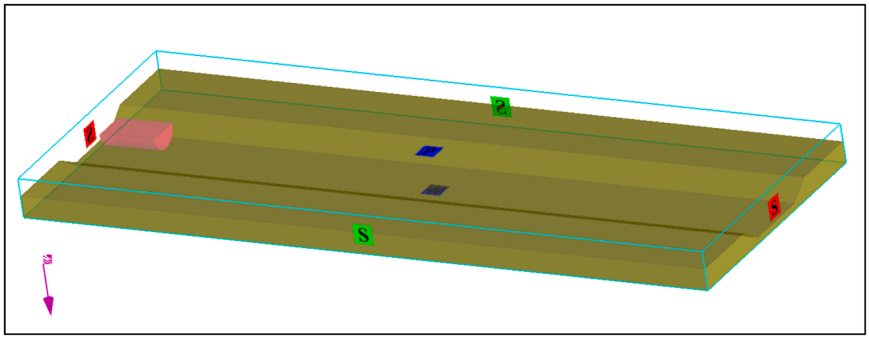

Fig. 4. Schematical view of the boundary conditions assigned to the numerical model.

4. Results and discussion

The results of the numerical simulations carried out in this study are assessed for the parameters of flow velocity and directions, bed shear stresses, suspended sediment concentrations and the morphological changes in the channel bed. Results are presented as graphics showing the values of these parameters at the end of the run time along the length of the channel.

The flow velocities for case S-1 at the end of the run time are presented in Fig. 5. It can be concluded from Figure X that the near-bed flow velocities (Fig. 5b) are greater than the velocities calculated at the free surface (Fig. 5a), mainly due to generation of motion induced currents around the hull of the barge. In both graphics, the increases in flow velocity at the bow of the barge and at the wake are obvious. Fig. 5c shows the distribution of flow velocities and directions between the x values 80 and 100 m over cross sections, spaced 4 m apart; again showing the increase in flow velocities at the bow and stern and also along the sides of the hull. The flow velocity distribution at the centreline is shown in Fig. 5d

Hydromorphologic changes and shear stresses for case S-1 are shown in Fig. 6. The spatial distribution of the suspended sediment concentration at the end of the run time is given in Fig. 6a. It can be observed that the maximum suspended sediment concentration value is at the wake of the barge with a maximum value of 150 kg/m^3. The amount of the suspended sediment concentration reduces with the distance from the barges stern, indicating a diffusion across the channel, i.e. in the y-direction. Fig. 6b shows the changes at the sea bottom surface due to sediment motion, displayed as deviations from the value of the undisturbed seabed. Variations up to 0.02 m in depth are observed at the centreline of the motin wakewards in terms of erosion, whereas accretions towards the channel banks are also evident. The shear stress distribution at the end of the run is shown in Fig. 6c and 6d, indicating that the highest values of the shear stress take place at the bow of the vessel with magnitudes rising to 15 Pa for this particular scenario. The bed shear stress drops rapidly along the barges hull sternwards, to a value of 3 Pa, and disperses further apart from the boat.

A comparative view of the distribution of free surface flow velocities and directions for four cases (S-1, S-2, S-5 and S-6) is given in Fig. 7. The width of the barge is constant ($B = 6.0$ m) for these cases. For the effect of tow speed, comparing Fig. 7a and 7b indicates that in both cases the flow velocities at the bow and wake of the vessel are greater than the tow velocity with a wake field extending further aft for the case Fig. 7a. The same conclusion can also be carried out by comparing Fig. 7c and 7d, where the only change is the bank slope (1:3 for S-1 and S-2 and 1:5 for S-5 and S-6). The effect of bank slope on flow velocities, on the other hand, is quite small.

A similar comparison for the suspended sediment concentrations has been presented in Fig. 8 for the same cases. In Fig. 8a and 8c, the tow speed is 1.5 m/s, whereas Fig. 8b and 8d show the cases with a tow speed of 1.0 m/s. By comparing Fig. 8a and 8b (or Fig. 8c and 8d), it can clearly be seen that the towing speed has a significant effect on the amount of the sediment moving into suspension. This is expected also as an outcome of the increased squat of the vessel, reducing the distance between the keel of the barge and the channel bed. Regarding the effect of bank slope, a slight reduction in suspended sediment concentrations for 1:5 sloped banks is observed when comparing cases S-1 and S-5 (or S-2 and S-6). The spatial distribution pattern of the suspended sediment concentrations are similar for both bank slope values.

Regarding the morphological changes taking place at the channel bottom, Fig. 9 has been summarized. Here, the morphological changes, i.e. accretions and erosions are shown as deviation values from the undisturbed channel bottom. While it can be concluded that similar spatial distributions are achieved for both 1:3 and 1:5 bank slope angles, i.e. by comparing Fig. 9a with 9b and Fig. 9c with

Table 1
Explanation of the scenarios used in the modelling.

Scenario	Barge width (m)	Barge Velocity (m/s)	Slope
S-1	6.0	1.5	1:3
S-2	6.0	1.0	
S-4	6.9	1.0	
S-5	6.0	1.5	1:5
S-6	6.0	1.0	
S-8	6.9	1.0	

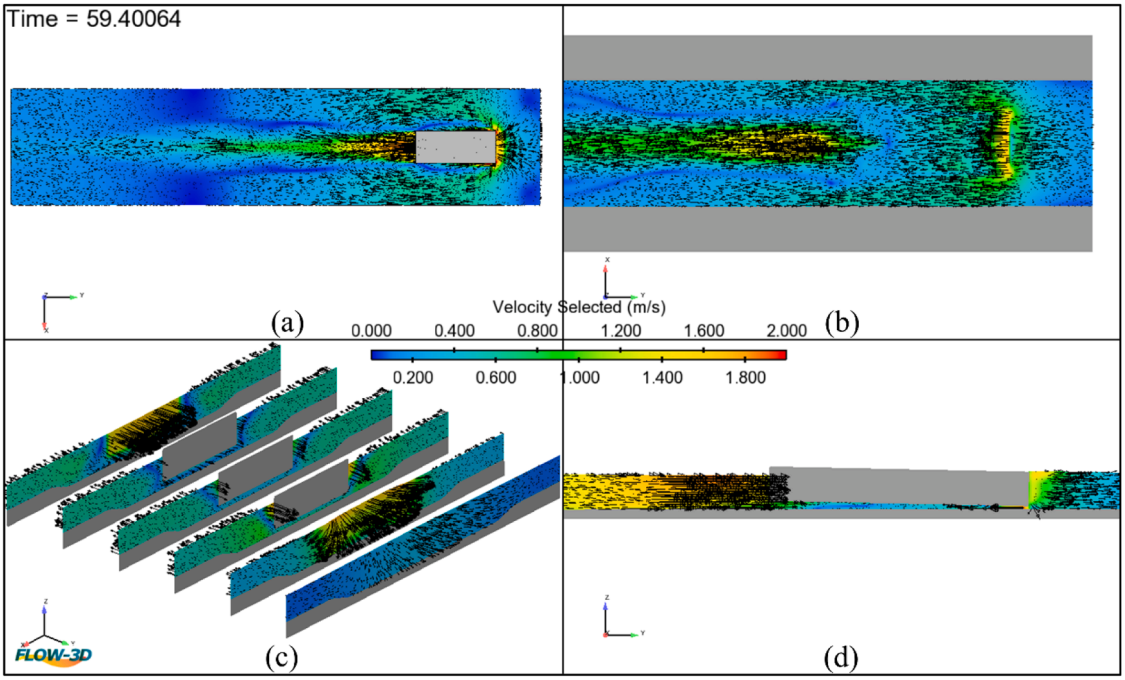

Fig. 5. Flow velocities and directions at the end of the run time for case S-1, (a) free surface (b) near-bed (c) cross sections along the barge spaced 4 m apart, between $x = 80$–100 m (d) profile view along the centerline, x-direction.

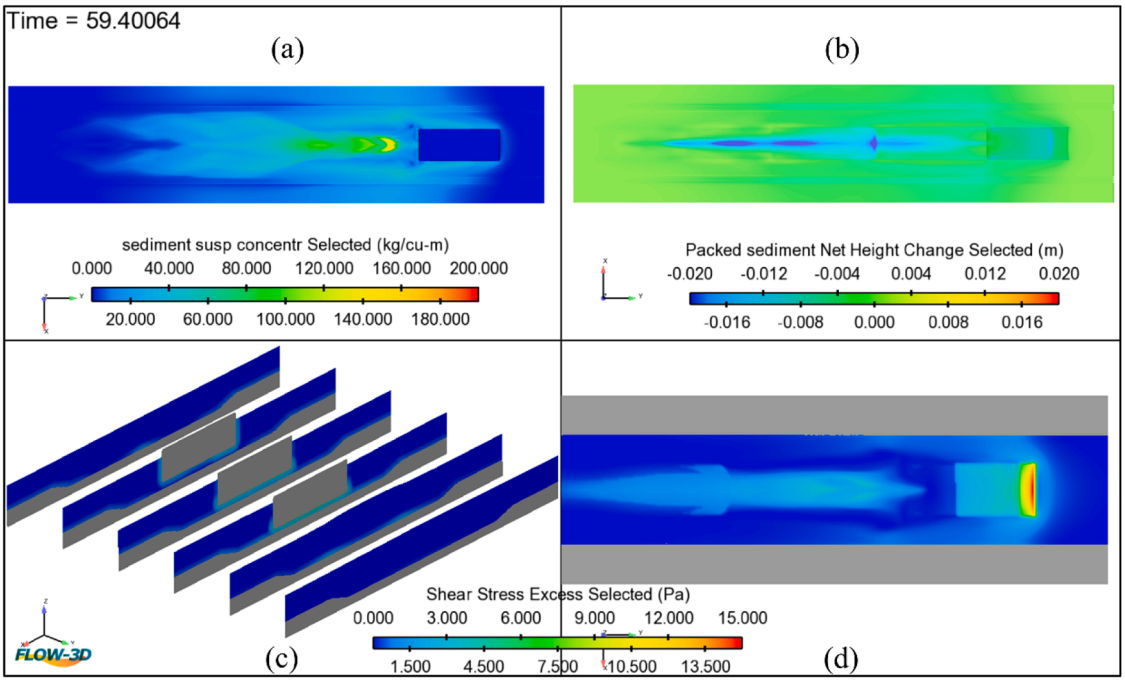

Fig. 6. Shear stresses and hydromorphologic changes for case S-1 at the end of the run time, (a) suspended sediment concentration, plan view (b) changes in bottom morphology, plan view (c) bottom shear stresses in cross sections spaced 4 m apart between $x = 80$ and 100 m (d) plan view of the bottom shear stress distribution.

9d, it can be observed that the width of the eroded region following the centreline of the barge increases for the smaller bank slope. The effect of towing speed is also obvious by comparing the Fig. 9a and 9c with Fig. 9b and 9d; the amount of erosion increases with increased tow speed.

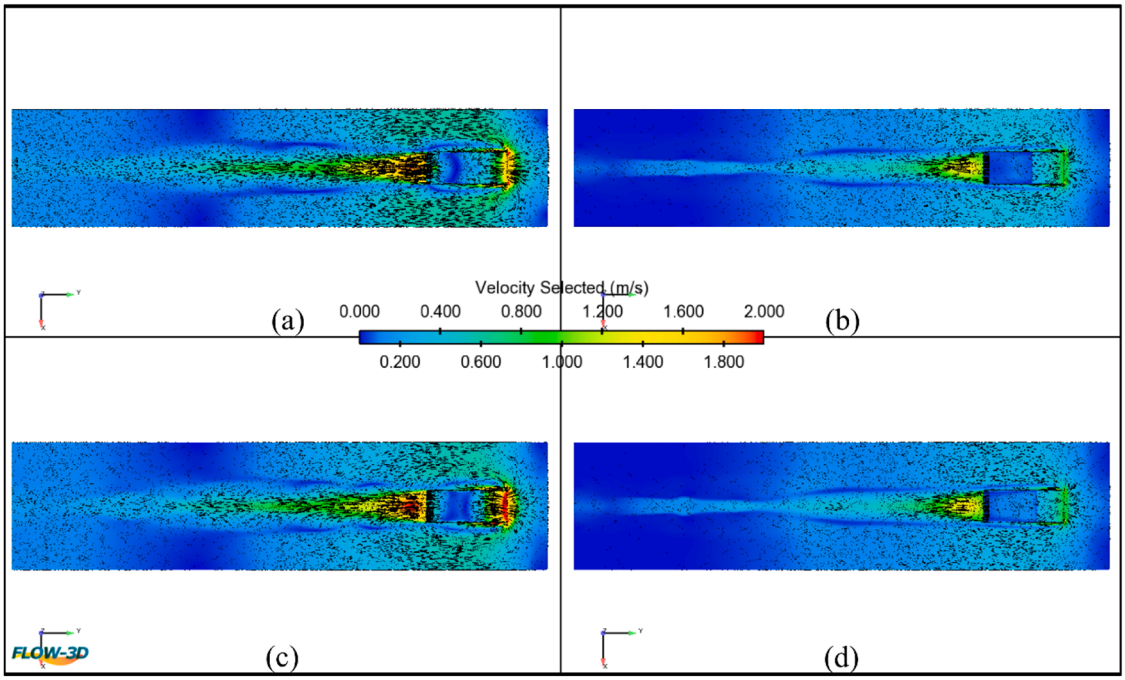

Fig. 7. Flow velocities at the free surface at the end of run time for different cases, (a) S-1 (b) S-2 (c) S-5 (d) S-6.

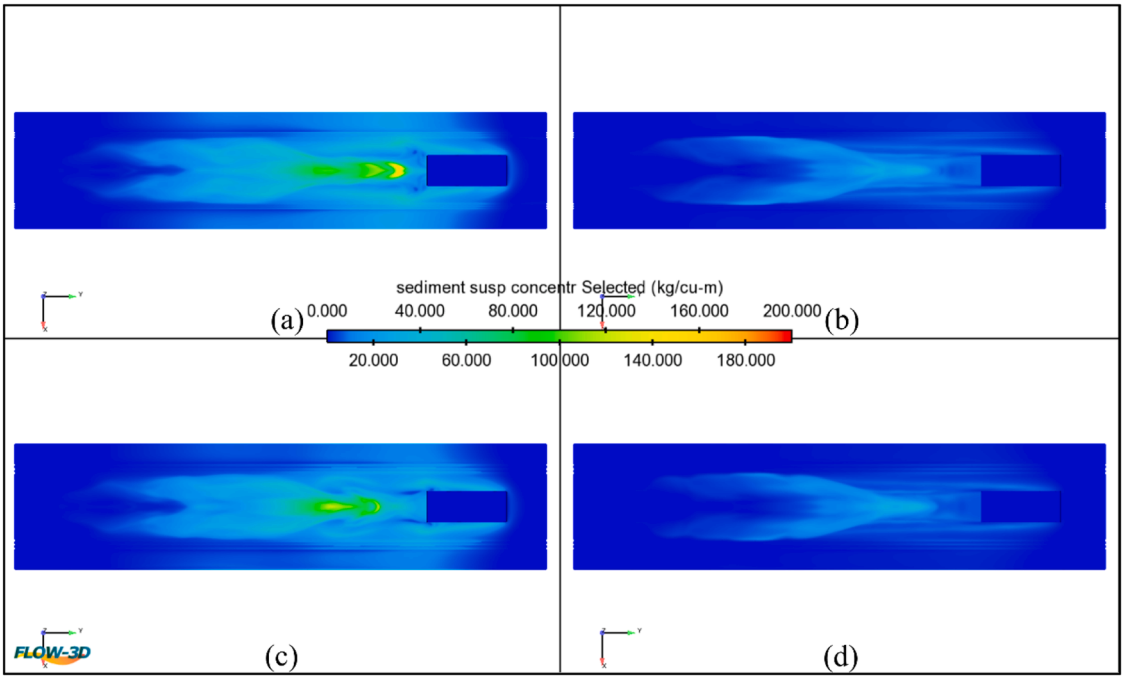

Fig. 8. Plan view of the suspended sediment concentrations at the end of run time, (a) S-1 (b) S-2 (c) S-5 (d) S-6.

A cumulative visualization of flow velocities at the free surface is given in Fig. 10 or cases with 1:3 bank slopes (S-1, S-2, S-4) and in Fig. 11 for cases with 1:5 bank slopes (S5, S6, S8). Here, one can observe that while the patterns for scenarios with equal tow speeds and boat widths, i.e. comparing S-1-S-5, S-2-S-6 and S-4-S-8, show similar spatial distribution patterns, the width of the area along the board boundaries of the vessel, where the tow-induced return currents take place, shows slightly smaller flow velocities for cases with 1:5 bank slopes. Flow velocities at the bow and stern also show similarities with maximum values reaching 2.0 m/s for cases S-1 and S-

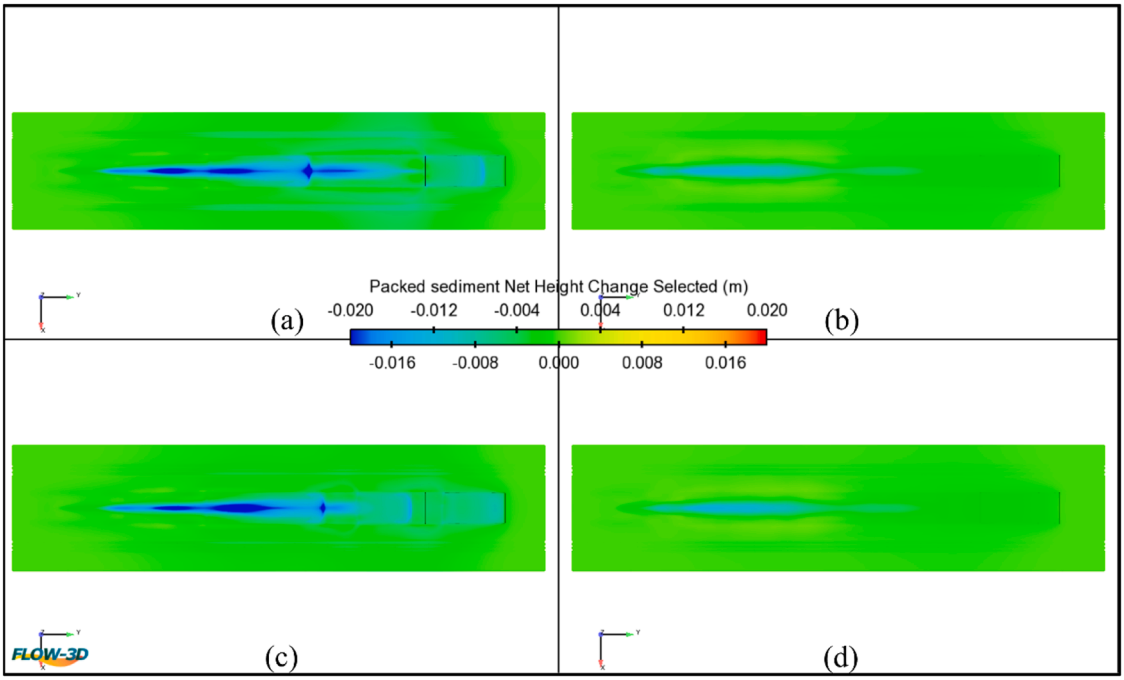

Fig. 9. Morphological changes at the channel bottom at the end of run time. Accretion and erosion values are given as deviation distances from the undisturbed bed. (a) S-1 (b) S-2 (c) S-5 (d) S-6.

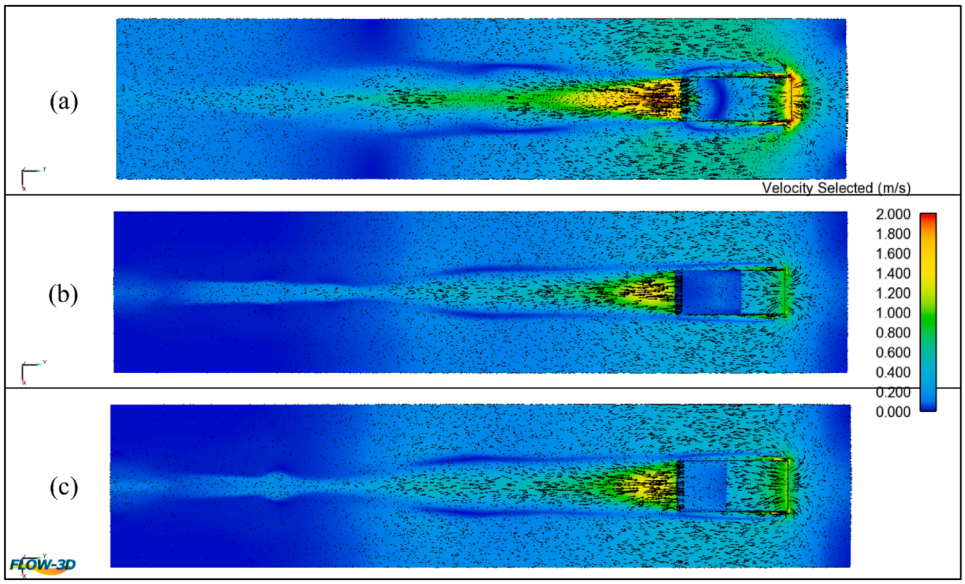

Fig. 10. Plan view of free surface flow velocities and directions at the end of run time, (a) S-1 (b) S-2 (c) S-4.

5 where the towing speed is 1.5 m/s; and 1.4 m/s for cases S2 and S6 at the bow, where the tow speed is 1.0 m/s. At the wake of the vessel, flow velocities are greater. It can also be observed that by increasing the width of the vessel to 6.9 m the altered flow velocity field grows in the y direction, while the change of flow velocities with respect to distance from the barges stern show similar behavior.

Changes in suspended sediment concentrations for different cases, namely for the cases compared in Figs. 10 and 11, are presented in Figs. 12 and 13, respectively, by taking the same case order into account. By comparing Fig. 12a and 12b or Fig. 13a and 13b, it is obvious that the tow speed significantly affects the amount of sediment suspension. The width of the vessel, on the other hand, also increases the amount of suspended sediment, clearly seen by comparing Fig. 12b and 12c or 13b and 13c. This is closely related to the increase in the displaced water volume at the bow of the vessel by increasing the vessels beam, leading to stronger return currents

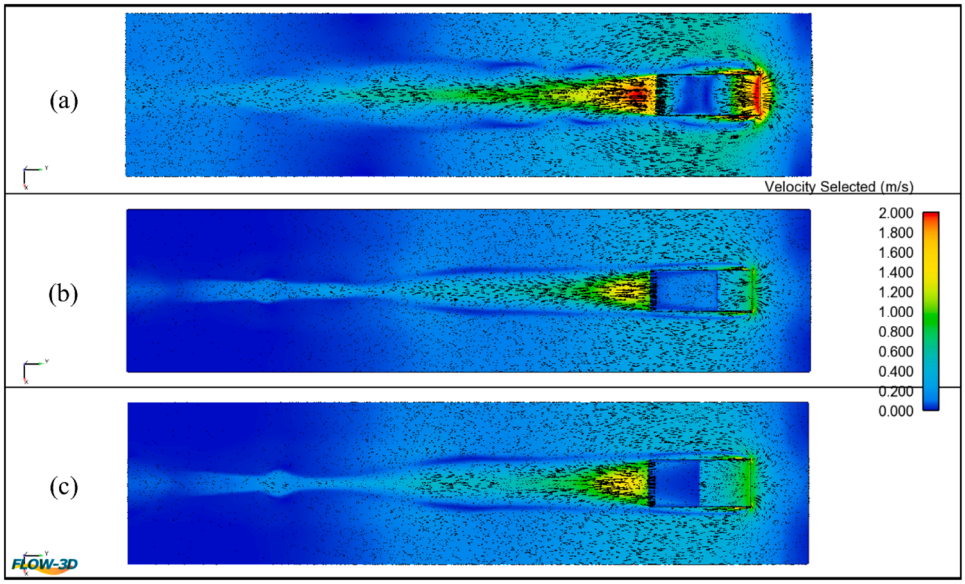

Fig. 11. Flow velocities and directions at the free surface, at the end of the run time, (a) S-5 (b) S-6 (c) S-8.

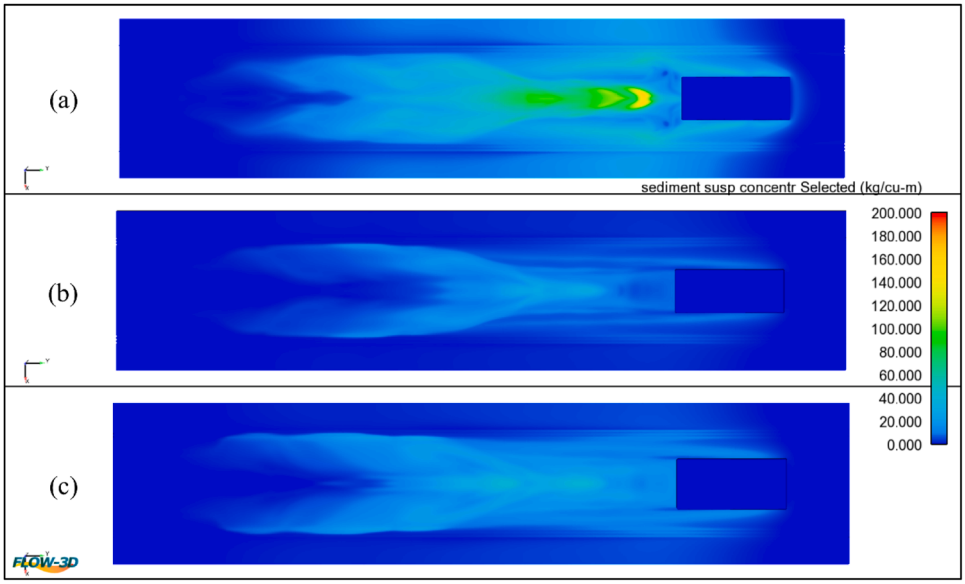

Fig. 12. Plan view of suspended sediment concentrations at the end of run time, (a) S-1 (b) S-2 (c) S-4.

acting in a larger flow field around the hull of the barge. The effect of bank slope, on the other hand, is relatively limited with respect to tow speed and vessel width, and by comparing Fig. 12 and Fig. 13 it can be found out that the spatial distribution of the suspended sediment differs slightly by changing the bank slope. In order to provide a better visualisation for tow speeds of 1.0 m/s, suspended sediment concentrations for cases S4 and S8 are given with a magnified scale in Fig. 14. It can be observed that sediment concentrations at the end of the run time are slightly greater for bank slopes of 1:3 with respect to bank slopes of 1:5, but retaining a similar spatial distribution pattern.

In order to evaluate a numerical comparison for the suspended sediment volumes, Figure N has been plotted, where the cumulative amount of suspended sediment has been plotted with respect to run time. From Fig. 15, it can be observed that the most significant parameter affecting the cumulative amount of suspended sediment is the tow speed. total amount of suspended sediment is slightly reduced for cases with 1:5 bank slopes than cases with 1:3 bank slopes. The amount of reduction in suspended sediment at the end of the simulation, is 14 % for cases with 6 m wide barges with a tow speed of 1.5 m/s, 14 % for cases with 6 m wide barges with a tow speed of 1.0 m/s and 15 % for cases with 6.9 m wide barges with a tow speed of 1.0 m/s. Thus, it can be concluded that a small amount

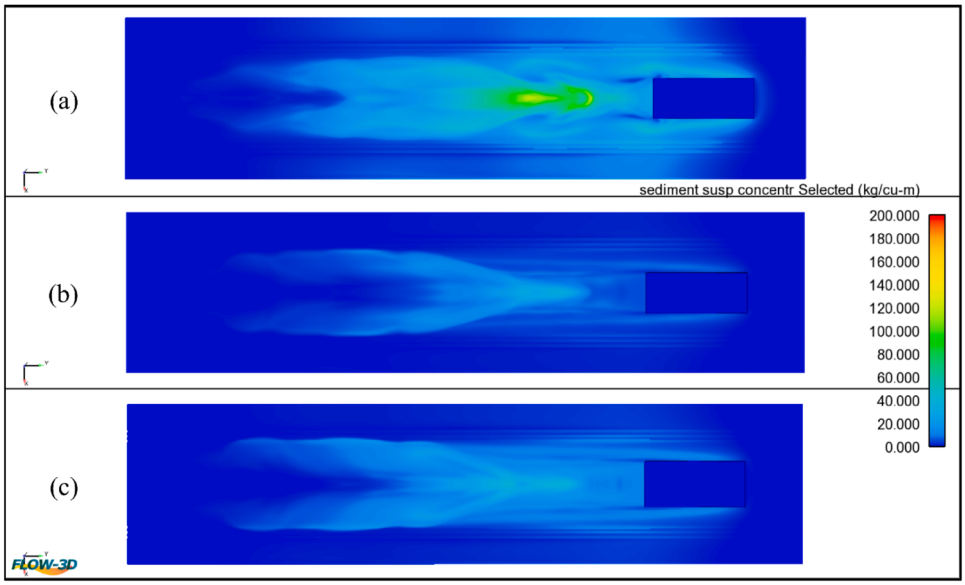

Fig. 13. Suspended sediment concentrations in plan view at the end of the run time, (a) S-5 (b) S-6 (c) S-8.

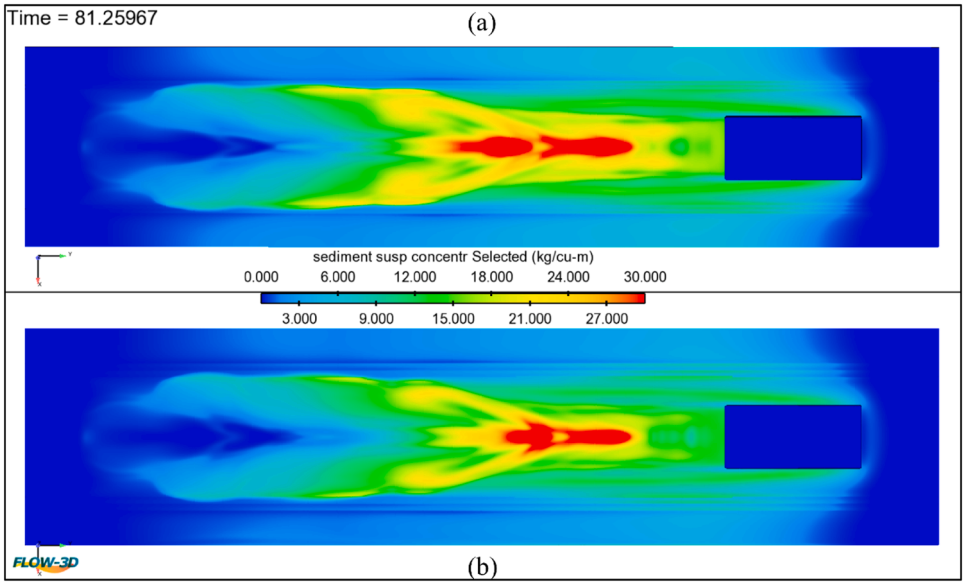

Fig. 14. Suspended sediment concentrations at the end of the run time, plan view, (a) S-4 (b) S-8. In order to visualize the difference better, the legend has been limited to 30 kg/m^3.

of reduction in sediment suspension can be achieved by using flatter bank slopes. Furthermore, for the same tow speed and draft, increasing the barges width 15 % leads to an increase in total suspended sediment; 72 % for 1:3 bank slopes and 66 % for 1:5 bank slopes. While the values are close for both bank slopes, further simulations are needed in order to evaluate a stable relationship.

The CFD simulations conducted using FLOW-3D Hydro reveal that vessel tow speed and hull width are the governing parameters in driving bed shear stress and subsequent sediment motion. This is consistent with findings from [21], who highlighted the critical role of return currents and hull geometry in generating sediment suspension. In line with [13] and [15], the present results confirm that increased flow velocities around the bow and stern of vessels are directly responsible for local peaks in sediment suspension.

The role of vessel beam width, often overlooked in field studies due to logistical limitations, was explicitly investigated in this study. A 15 % increase in vessel width resulted in up to a 72 % increase in suspended sediment volume, supporting the hypothesis proposed by [20] that larger vessels generate wider and more energetic wake fields that lead to a wider bed area in terms of sediment motion.

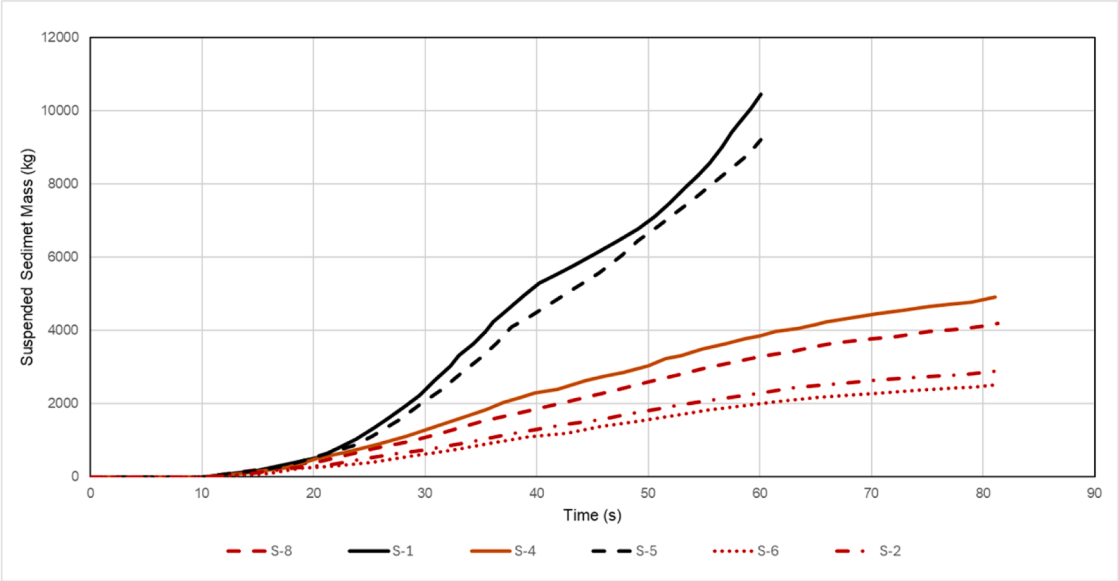

Fig. 15. Variation of the cumulative suspended sediment with respect to run time.

While many field studies such as those by [12] and [17] have emphasized the persistence of sediment in suspension following the passage of a vessel, the CFD-based approach in this study provides time-resolved insights into how such plumes originate and evolve spatially. Our simulations confirm that zones of high shear stress and erosion primarily align with the under-keel region and sidewalls of the hull, consistent with the physical model studies carried out by [24] and [25].

One novel aspect of the current work is the controlled isolation of bank slope as a variable, revealing that flatter bank slopes (1:5) resulted in a modest (~14–15 %) reduction in total sediment suspension. This finding introduces a quantifiable design parameter for future channel stabilization strategies, a topic often mentioned qualitatively in previous work but rarely explored through parametric modeling.

5. Conclusion

A numerical study has been carried out in order to inspect the effect of vessel motion on FLOW-3D Hydro commercial software has been used for the study. Simulations have been executed in a numerical flow region, 100 m long, 2 m deep and 22.0 m - 23.8 m wide. A grid has been assigned with 0.15 m x 0.15 m cell sizes, refining near the bottom to 0.0375 m x 0.0375 m. Two barge models with dimensions of $L_{OA} = 16$ m and $d = 1.6$ m have been modeled, which have different widths of $B = 6$ m and $B = 6.9$ m. Simulations have been carried out, following an accelerated ramp period, for two different constant towing speeds of 1.0 m/s and 1.5 m/s, and two different bank slopes, namely 1:3 and 1:5. A total of six cases have been simulated. Channel bed material is chosen as fine sand with a median diameter of 0.0625 mm and a specific density of 2650 kg/m^3. The corresponding critical Shields parameter and the amount of suspended sediment transport are calculated at each time step. Following results have been achieved:

- The near-bed flow velocities and hence the shear stress at the channel bottom receives its maximum value under the bow of the barge. Flow velocities are reduced towards the stern of the barge.
- The most significant parameter in affecting sediment motion and flow velocities is observed as the towing speed of the vessel, which is also proportional to the vessels squat value, triggering further reduction in the flow area under the hull and hence further increasing flow velocities and bottom shear stresses.
- Increasing the width of the vessel leads to the generation of a bow wave greater in displacement, it hence leads to an increase in flow velocities, reaching a peak value of 50 % under the keel for a tow speed of 1.5 m/s. This effect is diminished rapidly for the tow speed of 1.0 m/s. Bottom shear stresses are also consqeuently affected. The increase in vessel width also widens the zone where flow velocities are affected. A 15 % vessel width increase leads to a 72 % increase in the cumulative amount of suspended sediment.
- In all simulations, it has been observed that using smaller bank angles reduces the total amount of suspended sediment. For a change of bank slope from 1:3 to 1:5, a reduction of approx. 15 % in the cumulative amount of suspended sediment is observed. It also has been observed that morphological changes at the channel bottom are smaller in magnitude for smaller bank slope angles.

Funding

This work was supported by the Scientific Research Project Fund of Balikesir University under the project number: 2021/093.

Data availability

No data was used for the research described in the article.

References

[1] F. Ayaz, K. Heredağ, Fractional model for blood flow under MHD influence in porous and non-porous media, IJOCTA 14 (2) (2024) 156–167, https://doi.org/10.11121/ijocta.1497.
[2] H.A. Ali, M.R. Salman, Influence of rotation on peristaltic flow for pseudoplastic fluid: a wavy channel, IJOCTA 14 (4) (2024) 336–345, https://doi.org/10.11121/ijocta.1521.
[3] D. Avcı, B.B. İskender Eroğlu, N. Özdemir, Conformable fractional wave-like equation on a radial symmetric plate. In: Babiarz, A., Czornik, A., Klamka, J., Niezabitowski, M. (eds) Theory and Applications of Non-integer Order Systems. Lecture Notes in Electrical Engineering vol 407.
[4] UN Trade and Development (UNCTAD), 2024 Review of Maritime transport. https://unctad.org/publication/review-maritime-transport-2024, 2025 (accessed 3 April 2025).
[5] M. Briggs, M. Vantorre, K. Uliczka, P. Debaillon, Prediction of squat for underkeel clearance, in: Y.C. Kim (Ed.), Handbook of Coastal and Ocean Engineering, World Scientific Publishing Co. Pte. Ltd., 2009, pp. 723–774.
[6] PIANC, PIANC Report No. 121, PIANC, Brussels, Belgium, 2014.
[7] E.O. Tuck, Shallow-water flows past slender bodies, J. Fluid Mech. 26 (1966) 81–95.
[8] O. Bora, Ph.D. Thesis, Balikesir University Institute of Science, Balikesir, 2022.
[9] Navigation Channel Sedimentation Task Committee, Navigation channels and sedimentation. In: Kindle Edition, Navigation Channels and Sedimentation Soluitons (ASCE Manuals and Reports on Engineering Practice), American Society of Civil Engineers, https://doi.org/10.1061/9780784485149.
[10] T.M. Ravens, Ph.D. Thesis, Massachusetts Institute of Technology, Cambridge, MA, 1997.
[11] S.T. Maynord, Environmental Report 19, U.S. Army Corps of Engineers, Vicksburg, MS, USA, 2000.
[12] T.M. Parchure, W.H. McAnally, A.M. Teeter, Desktop method for estimating vessel-induced sediment suspension, J. Hydraul. Eng. 127 (2001) 577–587, https://doi.org/10.1061/(ASCE)0733-9429(2001)127:7(577).
[13] B.O. Bauer, M.S. Lorang, D.J. Sherman, Estimating boat-wake-induced levee erosion using sediment suspension measurements, J. Waterw. Port Coast. Ocean Eng. 128 (2002) 152–162, https://doi.org/10.1061/(ASCE)0733-950X(2002)128:4(152).
[14] J.A. McConchie, I.E.J. Toleman, Boat wakes as a cause of riverbank erosion: a case study from the Waikato River, New Zealand, J. Hydrol. N. Z. 42 (2003) 163–179.
[15] C. Houser, Sediment resuspension by vessel-generated waves along the Savannah River, Georgia, J. Waterw. Port Coast. Ocean Eng. 137 (2011) 246–257, https://doi.org/10.1061/(ASCE)WW.1943-5460.0000088.
[16] B.K. Eriksson, A. Sandström, M. Isæus, H. Schreiber, P. Karås, Effects of boating activities on aquatic vegetation in the Stockholm archipelago, Baltic Sea, Estuar. Coast. Shelf Sci. 61 (2004) 339–349, https://doi.org/10.1016/j.ecss.2004.06.019.
[17] J. Rapaglia, L. Zaggia, K. Ricklefs, M. Gelinas, H. Bokuniewicz, Characteristics of ships' depression waves and associated sediment resuspension in Venice Lagoon, Italy, J. Mar. Syst. 85 (2011) 45–56, https://doi.org/10.1016/j.jmarsys.2010.11.005.
[18] L. Zaggia, G. Lorenzetti, G. Manfé, G.M. Scarpa, E. Molinaroli, K.E. Parnell, J.P. Rapaglia, M. Gionta, T. Soomere, Fast shoreline erosion induced by ship wakes in a coastal lagoon: field evidence and remote sensing analysis, PLoS One 12 (2017) e0187210, https://doi.org/10.1371/journal.pone.0187210.
[19] G. Duró, A. Crosato, M.G. Kleinhans, D. Roelvink, W.S.J. Uijttewaal, Bank erosion processes in regulated navigable rivers, J. Geophys. Res. Earth Surf. 125 (2020) e2019JF005438, https://doi.org/10.1029/2019JF005438.
[20] L. Mao, Y. Chen, Investigation of ship-induced hydrodynamics and sediment suspension in a heavy shipping traffic waterway, J. Mar. Sci. Eng. 8 (2020) 424, https://doi.org/10.3390/jmse8060424.
[21] S. Ji, A. Ouahsine, H. Smaoui, P. Sergent, 3D numerical modeling of sediment resuspension induced by the compounding effects of ship-generated waves and the ship propeller, J. Eng. Mech. 140 (2014) 04014034, https://doi.org/10.1061/(ASCE)EM.1943-7889.0000743, 140.
[22] S. Ji, A. Ouahsine, H. Smaoui, P. Sergent, 3D modeling of sediment movement by ships-generated wakes in confined shipping channel, Int. J. Sediment Res. 29 (2014) 49–58, https://doi.org/10.1016/S1001-6279(14)60029-3.
[23] J. Du, J. Wong, G. Li, Ship-induced sediment suspension in the Changjiang Estuary, J. Coastal Res. 70 (2014) 167–172, https://doi.org/10.2112/SI70-029.1.
[24] T. Robijns, Master's Thesis, Delft University of Technology, Delft, The Netherlands, 2014.
[25] M. Schroevers, K.D. Berends, T. Vermaas, H.J. Verheij, Measuring ship-induced currents in a canal, in: Proc. of the 2015 826 IEEE/OES 11th Current, Waves and Turbulence Measurement (CWTM), St. Petersburg, FL, USA, 2015, pp. 2–7, https://doi.org/10.1109/CWTM.2015.7098126, 2–6 March.
[26] M.J.B. da Silva, I.C.S. Correa, J.A.S. Fontoura, C.G. Serpa, Sedimentation processes in the navigation channel of Patos Lagoon Estuary, southern Brazil, Reg. Stud. Mar. Sci. 61 (2023) 102931, https://doi.org/10.1016/j.rsma.2023.102931.
[27] A.C. Muscalus, K.A. Haas, Vessel wake contributions to erosion at exposed and sheltered shorelines near a tidal shipping channel, Coastal Eng. 178 (2022) 104220, https://doi.org/10.1016/j.coastaleng.2022.104220.
[28] C. Colangeli, G. Leftheriotis, A. Dimas, M. Brocchini, Ship-forced sediment transport: a new model for propeller jet flow, Water 16 (12) (2024) 1647, https://doi.org/10.3390/w16121647.
[29] N. Gedik, O. Bora, M.S. Kabdaşlı, E. Irtem, Hydrodynamic and morphological effects of non-powered floating objects on sediment resuspension: a CFD and regression analysis, Appl. Sci. 15 (2025) 2717, https://doi.org/10.3390/app15052717.
[30] FLOW-3D® HYDRO Version 1.0 Users Manual. FLOW-3D [Computer Software], Flow Science, Inc., Santa Fe, NM, 2020.
[31] V. Yakhot, L.M. Smith, The renormalization group, the ε-expansion and derivation of turbulence models, J. Sci. Comput. 7 (1) (1992) 35–61, https://doi.org/10.1007/BF01060210.
[32] D.R. Mastbergen, J.H. Van Den Berg, Breaching in fine sands and the generation of sustained turbidity currents in submarine canyons, Sedimentology 50 (4) (2003) 625–637.
[33] R. Soulsby, Bedload transport, in: R. Soulsby (Ed.), Dynamics of Marine Sand, Thomas Telford Publications, London, 1997, pp. 155–170.
[34] C.W. Hirt, B.D. Nichols, Volume of fluid (VOF) method for the dynamics of free boundaries, J. Comput. Phys. 39 (1981) 201–225, https://doi.org/10.1016/0021-9991(81)90145-5.